Direct-Write Photolithography for Cylindrical Tooling Fabrication in Roll-to-Roll Microcontact Printing

Larissa F. Nietner
Laboratory for Manufacturing and Productivity,
Massachusetts Institute of Technology,
Room 35-131,
Cambridge, MA 02139
e-mail: nietner@mit.edu

David E. Hardt[1]
Fellow ASME
Laboratory for Manufacturing and Productivity,
Massachusetts Institute of Technology,
Room 35-231,
Cambridge, MA 02139
e-mail: hardt@mit.edu

Direct-Write Photolithography for Cylindrical Tooling Fabrication in Roll-to-Roll Microcontact Printing

The scale-up of microcontact printing (μCP) to a roll-to-roll technique for large-scale surface patterning requires scalable tooling for continuous pattern printing with μm-scale features (e.g., 1–50 μm). Here, we examine the process of creating such a tool using an optical direct-write or "maskless" method working on a rotating cylindrical substrate. A predictive model of pattern formation is presented along with experimental results to examine the key control factors for this process. It is shown that factors can be modulated to vary the cross-sectional shape in addition to feature height and width. This feature can then be exploited to improve the robustness of the final printing process.
[DOI: 10.1115/1.4030766]

Introduction

μCP can achieve submicrometer-scale patterns as small as 30 nm [1,2], but scale-up to production at high rates (∼1 m/s web speed) and large areas (>0.5 m web width) is yet to be achieved. There is considerable interest in roll-to-roll configurations for this purpose, and the essential element in this process is creation of cylindrical image carriers or "stamps" for this process. One approach to this is to wrap a flat stamp around a printing mandrel [3–7], but this presents limitations for size and thickness uniformity and creates a noncontinuous cylinder. Master patterns are usually formed on silicon wafers, but wafer sizes are limited, thus presenting difficulty for scaling the process. There are methods for casting larger area μCP stamps (see, e.g., Ref. [5]), but these result in low absolute accuracy and have not been fully developed. Additionally, any method that requires the wrapping of a flat-cast stamp around a cylinder will result in pattern deformation, residual stresses, and an inevitable discontinuity in the pattern. Though a stamp can be cut to proper size for wrapping, any deviation at the seam between its ends will result in a significant once-per-revolution disturbance that might preclude any reliable printing of μm-sized features at medium-to-high speeds. Finally, the stamp accuracy strongly depends on the mounting process, and none of the available mounting processes is sufficiently accurate for mounting large stamps without causing pattern distortions or thickness variations.

To address these problems, Petrzelka and Hardt [8] developed a method for the fabrication of seamless cylindrical stamps for μCP using a centrifugal casting method. In this method, a cylindrical master pattern is created by a laser direct-write process on a positive photoresist spun to even thickness within the centrifuge. Possible eccentricity and roughness are eliminated by a planarizing layer of flood-cured SU-8 photoresist on the cylinder surface, which forms a smooth substrate for the patterning layer. The centrifugal force produced by the spinning drum provides for even spreading of both the photoresist master pattern and the polydimethylsiloxaone (PDMS) precursors during casting throughout the interior surface of the drum. This approach produces continuous cylindrical tools of very uniform thickness, is scalable beyond current size limits, and does not require an additional mask creation step for changes in pattern geometry. As such, it was the first process to produce a seamless cylindrical stamp of consistent uniformity with micrometer-scale features (an example is shown in Fig. 1). The method was demonstrated in an initial proof of concept. The achievable aspect ratios, smooth topology, and micrometer-scale resolution of the pattern combined with the scalable cylindrical layout render this method highly suitable for creating continuous cylindrical stamps. However, the range of features shapes and the key process factors that determine these remain unexplored.

This paper extends this novel casting method by examining the laser patterning process in detail. In addition to feature location and feature size, the process is characterized by the cross-sectional geometry produced. While the former two factors determine where pattern transfer will occur in printing, the latter is crucial to feature stability when subjected to contact pressures, and therefore determines the precision limits and area robustness of the printing step. As shown by Petrzelka and Hardt [9], feature collapse, and therefore printing failure, can occur whenever local pressure exceeds the mechanical limits of the features. Since feature collapse can occur by buckling, over-compression, or

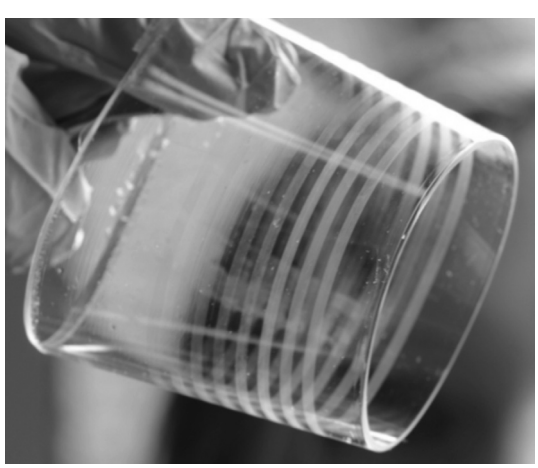

Fig. 1 A centrifugally cast tool with circumferential features of 25 μm width at 100 μm pitch arranged within bands of 20 lines each

[1]Corresponding author.

Contributed by the Manufacturing Engineering Division of ASME for publication in the Journal of Micro- and Nano-Manufacturing. Manuscript received February 10, 2015; final manuscript received June 1, 2015; published online June 25, 2015. Assoc. Editor: Sangkee Min.

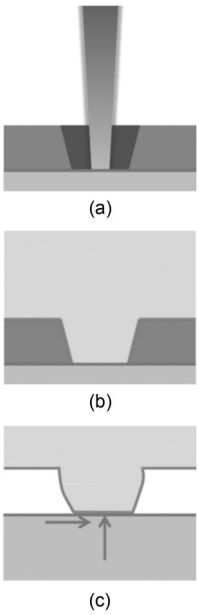

Fig. 2 Schematic of the process sequence. (*a*) The laser-resist patterning step determines the shape of the stamp feature in the positive resist. (*b*) The centrifugal casting of the PDMS stamp. (*c*) The resulting stamp feature, which in the printing process has to withstand normal pressure with the substrate required to transfer ink, capillary forces, and van der Waals interactions with adjacent feature surfaces.

collapse of the space between features, changes in the cross section will directly affect these stability limits. In addition, the cross section can influence the ink transfer behavior and influence how much print force is required to ensure conformal contact. A schematic of this process sequence is shown in Fig. 2.

The process of direct-write photolithographic patterning in this context is examined both analytically and experimentally to create a model that can predict the geometry of features given a specific photoresist and laser geometry. In so doing, the range of achievable geometries is explored, and the parameters that produce a cross-sectional geometry for more stable stamp features are determined.

Feature Geometry and Process Robustness

Beyond scale-up and cylindrical continuity, a critical factor in μCP stamps is the sensitivity of the printing process to contact pressure variations given the stamp feature collapse modes [9–12].

PDMS is the stamp material of choice for μCP because it replicates the master pattern with nanometer-resolution, allows for diffusive substance transfer, and it can achieve conformal contact over a wider range of surface asperities [13].[2] However, the high compliance of PDMS also leads to a variety of error modes, such as feature bulging, lateral buckling, or roof collapse (collapse of the region in between features). These are shown in Fig. 3. The common factor for these error modes is the mechanical response of the feature to printing forces [9], van der Waals interactions, and capillary forces [14], where the material's elasticity is required for ensuring conformal contact with the substrate [15]. Resulting PDMS surface interaction forces were derived by Chaudhury and Whitesides [16] and demonstrated for lines-and-spaces patterns by Delamarche et al. [12].

[2]The ratio of surface energy γ_s (about 20 mJ/m^2) to elastic modulus E_0 (about 2 MPa) for conventional Sylgard 184 PDMS is quite large. The material radius of curvature $\rho_m = \gamma_s/E_0$ is thus on the order of 10 nm. The surface energy has a significant effect at this length scale and permits conformal contact over a substrate with a surface roughness on the order of ρ_m.

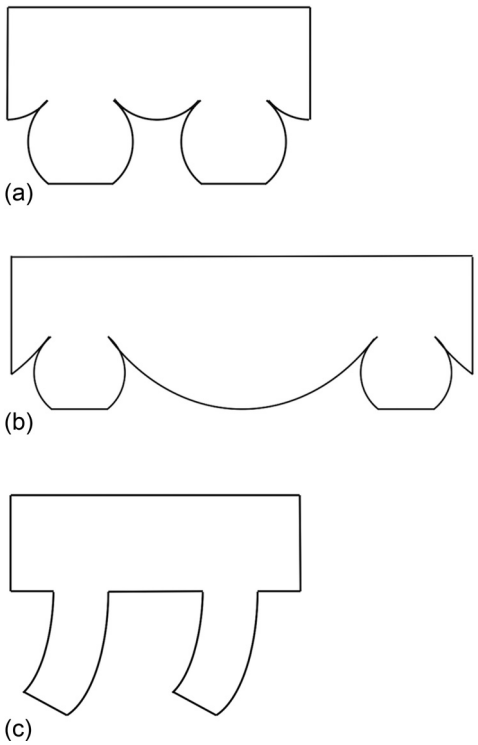

Fig. 3 Stamp feature deformation modes: (*a*) sidewall collapse, (*b*) roof collapse, and (*c*) buckling

These defects can be minimized by modifying the geometry of the stamp features. Menard and Rogers [17] suggest pursuing aspect ratios between approximately 0.05 and 2 to reduce the risk of collapse or sag, but they did not investigate effects of the detailed cross-sectional geometry. By contrast, Hizir et al. [18] showed that slanted feature sidewalls can significantly increase the robustness of the tool to print force variation, while also minimizing the increase in contact area as print pressure increases.

As shown in Fig. 2, the cross-sectional geometry of the stamp features in the presented process is determined by the photolithographic step. Hence, for scaling μCP to produce large stamps with complex patterns, understanding the photolithographic exposure process factors that determine the detailed dimensions of the pattern is critical.

The work presented here applies the Dill process model [19] to describe the intracylindrical laser direct-write lithography on a thick resist film. Furthermore, it empirically determines the robustness to process variations, such as exposure intensity, resist film thickness, and writing speeds. In examining the boundaries of the photolithographic process, feature geometries are discovered that can be highly beneficial to a robust printing process.

A Spatial and Temporal Model of Resist Conversion

Initial experiments with SPR 220 and AZ 9260, two similar positive-tone photoresists, demonstrated that varying thicknesses and exposure times could yield a variety of feature sizes and shapes. To understand these effects, a two-dimensional (2D) model of both the input laser intensity and the resulting local and temporal photoresist state was implemented to guide and extend the ensuing experiments.

The fraction of the remaining photoactive compound (PAC) at a given location in the resist determines where material dissolves upon development after exposure. A diazonaphthoquinone (DNQ)-based positive photoresist, such as SPR 220 or AZ 9260, is rendered dissolvable through ultraviolet irradiation in a nonlinear fashion. Upon exposure, DNQ (the PAC) is converted into base-soluble indene acid. The distribution of this state in the 2D

model is shown in Fig. 4 as the remaining concentration $M(x,y,t)$, which ranges from one for completely unexposed resist and zero for completely exposed resist. This figure further shows the model of the light source, a Gaussian intensity distribution, which impinges on the photoresist.

Analytical Model. A classical model of this process was developed by Dill et al. [19]. In this model, the rate of resist conversion is given by

$$\frac{\partial M(x,y,t)}{\partial t} = -I(x,y,t)M(x,y,t)C \tag{1}$$

where $I(x,y,t)$ *is* the local light intensity, and C is the sensitivity of the photoresist that determines how fast the material reacts to the light.

As the incident light penetrates the resist, the ultraviolet absorption of the reaction products is much less than that of the unexposed PAC. This effect must be considered when dealing with resist layer thicknesses in the range of 1–50 μm as is typical for stamp casting. These optical properties cause nonlinear light propagation, also referred to as contrast, and thus affect the shape of the resulting cross section. Dill's model describes this process algebraically as shown in Eq. (2). In this relationship, the absorption coefficient α for any time and location in the resist is defined through parameters A and B as a function of the quantity M

$$\alpha(x,y,t) = A*M(x,y,t) + B \tag{2}$$

Values for A and B describe the absorption coefficient before, during, and after exposure, where $A+B$ is the absorption coefficient of unexposed resist, and B is the absorption coefficient of fully exposed resist.

By applying the Beer–Lambert law [20] and incorporating the absorption relationship of Eq. (2), the intensity at any location $I(x,y^*)$ at any time t during the exposure process is given by

$$I(x,y^*,t) = I_0(x)*\exp\left(-\int_0^{y^*}(A*M(x,y,t)+B)dy\right) \tag{3}$$

where $I_0(x)$ is the intensity distribution of the focused beam on the photoresist surface. This distribution then depends on the specific light source in use.

The intensity distribution of the focused diode laser used in the apparatus is modeled as a Gaussian distribution [21,22], and in the 2D reference frame of Fig. 4 this is simplified to

$$I(x,y) = I_0\left(\frac{\omega_0}{\omega(y)}\right)^2 e^{-\frac{2x^2}{\omega^2(y)}} \tag{4}$$

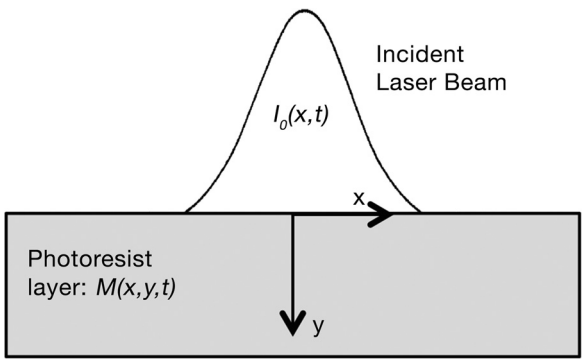

Fig. 4 Model layout showing cross section of resist with the photoresist state $M(x,y,t)$ and input intensity $I_0(x)$

where the half-width of the beam, $\omega(y)$, at longitudinal positions y is limited by the light's wavelength λ and the beam half-width at its waist, ω_0

$$\omega^2(y) = \omega_0^2\left(1+\left(\frac{y\cdot\lambda}{\pi\cdot\omega_0^2}\right)^2\right) \tag{5}$$

The width of the beam at the focal point is $2\omega_0$. This is defined as the distance between the two locations with an irradiance of I_0/e^2 across the transverse direction of the beam at the focal point, where the irradiance in the center of the beam equals I_0.

For the 2D simulations, only the distribution at the focal point is considered, yielding the equivalent intensity

$$I(x) = I_0 e^{-\frac{2x^2}{\omega_0^2}} \tag{6}$$

The laser peak intensity can be calculated from the laser power P if the focused beam width ω_0 is known

$$I_0 = \frac{2P}{\pi\omega_0^2} \tag{7}$$

The total dose in the model is modulated by exposure time, and in the experiments by writing speed, both assuming a fixed overall power P.

Parameters A and B for the positive-tone photoresists SPR 220 and AZ 9260 were found in the material specifications given by the manufacturers. Parameter C was estimated from the provided thickness-dose-examples using the following relationship from Mack [23]:

$$C = \frac{A+B}{AT_0(1-T_0)T_{12}}\left.\frac{dT}{dE}\right|_{E=0} \tag{8}$$

where $(dT/dE)|_{E=0}$ is the initial slope of the transmittance-dose curve, and T_0 and T_{12} are the initial resist transmittance and air-resist transmittance, respectively. The parameters used for the simulations are summarized in Table 1.

Numerical Solution. The above relationships can be combined to create a model of the spatial distribution of remaining PAC ($M(x,y,t)$) given the laser input distribution, absolute intensity, and exposure time. A numerical simulation was created in MATLAB by discretizing the cross section and creating two matrices; one for $I(x,y,t)$ and one for $M(x,y,t)$. Values were updated through nested loops to simulate the progression of the exposure process. The initial condition for the material mesh is $M=1$ for all locations, indicating a fully unexposed resist.

The exposure intensity at the mesh boundary was modeled as Gaussian beam (as per Eq. (6)) with input parameters for focused beam waist width ω_0, wavelength λ, and laser power P. The exposure intensity in the material below the first mesh layer was calculated using Eq. (3).

The local PAC concentration remaining after each exposure loop interval was applied in calculating the subsequent intensity at each mesh point for the next loop, following Eq. (2). The spatial and temporal resolutions of these calculations were chosen to

Table 1 *A*, *B*, and *C* parameters for the photoresists in simulating the exposure process

Parameter	SPR 220	AZ 9260	Units
A	0.71	0.36	μm^{-1}
B	0.02	0.01	μm^{-1}
C	0.017	0.005	cm^2/mJ

match the expected feature sizes and ensure a stable yet efficient numerical integration. For the simulation results presented here, these were 1 μm and 1 ms, respectively.

Simulation Results. The illumination properties were chosen to match the experimental apparatus ($P = 80$ mW, $\omega_0 = 5\,\mu$m, and $\lambda = 405$ nm), and the simulation was executed over a number of thicknesses and duration levels for both SPR 220 and AZ 9260. Typical results for a resist thickness of 10 μm are shown in Fig. 5 for SPR 220 and Fig. 6 for AZ 9260. Each figure shows how the fraction of PAC changes with continuous exposure and how the cross section develops. Moreover, it shows differences between the resulting cross sections. In Fig. 5, the resulting feature has highly sloped sidewalls, whereas in Fig. 6, the resulting sidewalls are nearly vertical. This phenomenon is caused by the differing contrast of the two resists. SPR 220 can be considered a medium contrast resist when compared to AZ 9260. SPR 220 is initially more absorbent, and light cannot easily penetrate deeply into unexposed material, therefore a Gaussian light source creates sloped sidewalls. AZ 9260, which has a higher contrast, allows more light to penetrate the resist without absorption, and thus creates steeper sidewalls.

Experiments

Scope. An extensive set of experiments was performed to determine the stamp feature cross section for a given set of exposure parameters for both photoresists. The parameters included the thickness of the photoresist layer and the exposure dose per unit of surface area (modulated via the centrifuge rotation speed). The apparatus that formed the base for these experiments, as developed by Petrzelka and Hardt [8], is shown in Fig. 7. To avoid

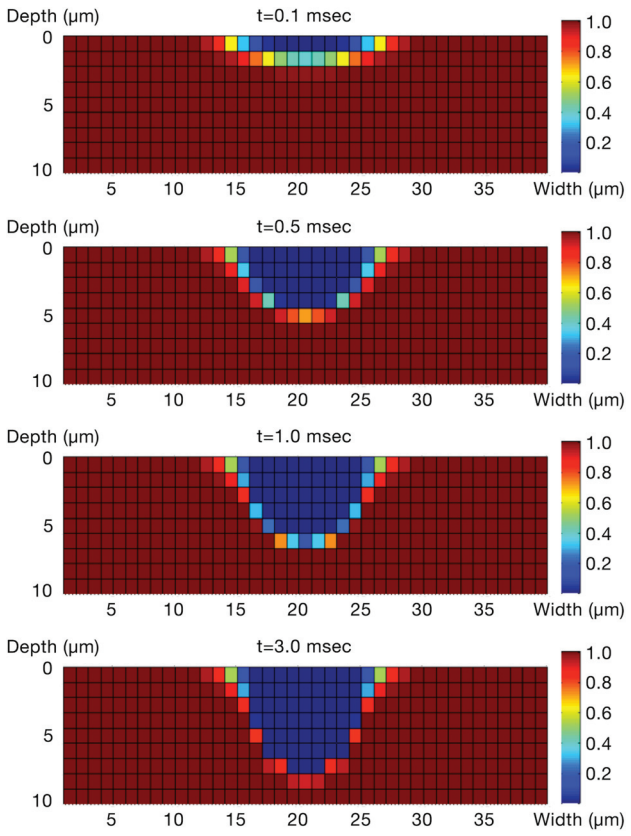

Fig. 5 Result of the simulation for SPR 220. Exposure durations $t = t_0 + 1, t_0 + 5, t_0 + 10$, and $t_0 + 30$ in 0.1 ms intervals. Concentration of remaining PAC is shown by color. Note the highly sloped sidewall prediction.

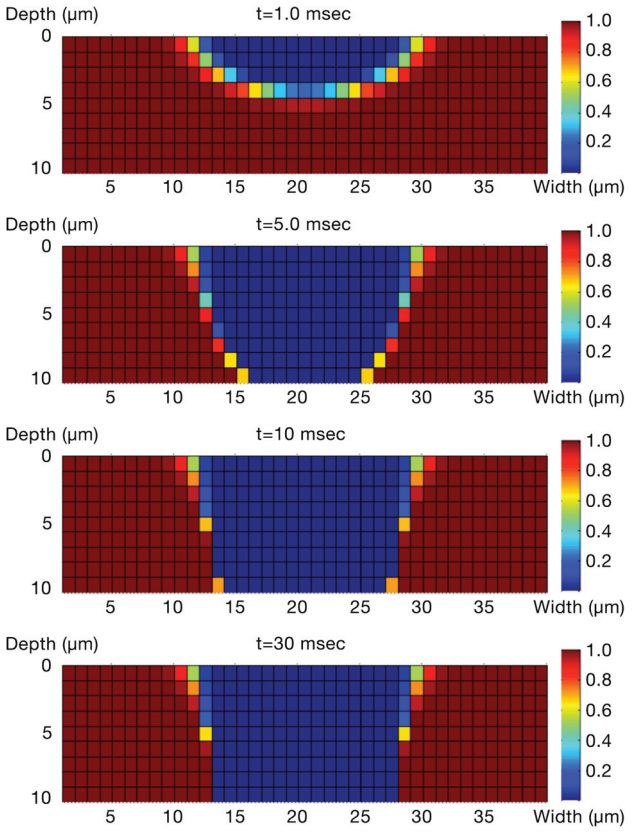

Fig. 6 Result of the simulation for AZ 9260. Exposure durations $t = t_0 + 1, t_0 + 5, t_0 + 10$, and $t_0 + 30$ in 1 ms intervals. The simulation showed nearly straight sidewalls, as the low absorption attenuates light less significantly when passing through the material.

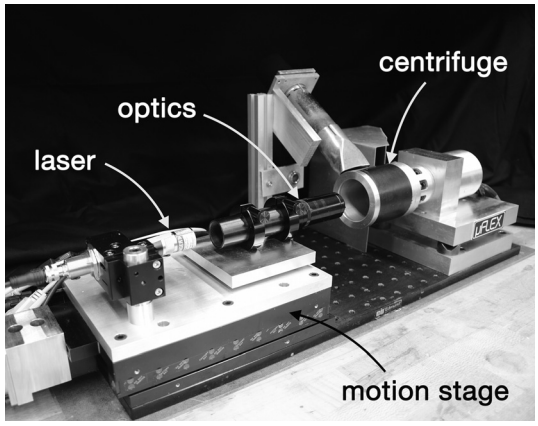

Fig. 7 The system comprises a laser with focusing optics, mounted on a linear axis, which can write on the inside of a drum that serves as a centrifuge for casting the tools

errors related to the axial motion of the laser parallel to the substrate and to ensure constant rotation speeds, only circumferential lines were written. The laser was actuated as a function of the radial position of the drum once the writing speed was reached, ensuring constant writing speed over one exact rotation. Postexposure baking steps, development temperature and development time were kept constant to ensure reproducibility of the threshold PAC concentration causing removal of the resist upon development.

Measurements were taken at an arbitrary angular position of the drum and 120 deg to either side for three data points per rotation,

which allowed for an analysis of the taper and eccentricity of the drum. The cylinder was divided into several sections, and the same pattern was repeated in every section to account for possible coaxial deviation between the substrate and the optics trajectory. Within each section, an array of writing speeds was sampled with multiple turns per speed as outlined in Fig. 8.

The complete experiment was repeated for different resist thicknesses by casting a new resist layer each time. The range of thicknesses spanned 10–25 μm for AZ 9260, as recommended by the manufacturer, and 1.5–10 μm for SPR 220. Given a constant laser power and spot size, the variation in writing speed corresponded to a variation in exposure dose per unit surface area, which produced different feature dimensions in the photoresist master for different layer thicknesses. As will be noted later, the intensity distribution was subject to a transverse dislocation of the laser focal point, caused by deviation in parallelism of the laser traverse axis and the rotational axis.

The full set of experimental combinations is displayed in Fig. 9, and the experiments were conducted following the protocol given in Nietner [24].

Measurement Methods. To measure the pattern geometries, PDMS tools cast on the patterns were subsequently sectioned and measured. The cast parts were sectioned longitudinally using a razor blade at three evenly spaced circumferential locations. The cross-sectional geometries of the features were observed using conventional optical microscopy, a white light interferometer, and an environmental electron microscope (ESEM). In the optical microscope (LW Scientific, Lawrenceville, GA), the sectioned tools were projected on a CCD camera (9.6 pixel/μm using a 40× objective). The cross section was characterized by its top width (the effective print feature width), its root width, and by its height and sidewall angle. These attributes are illustrated in Fig. 10. A typical result for AZ 9260 as observed using the microscope and ESEM is shown in Fig. 11.

Experimental Results. Both resists exhibited a large range of top width, root width, and sidewall angle characteristics. With increasing writing speed, the power dose per unit surface area decreases, resulting in smaller features. A threshold effect was seen in thin films where the resist exhibits a high contrast, which is typical of conventional photolithography. The required power dose for a given film thickness was in accordance with recommendations given by the photoresist manufacturer, and as predicted by

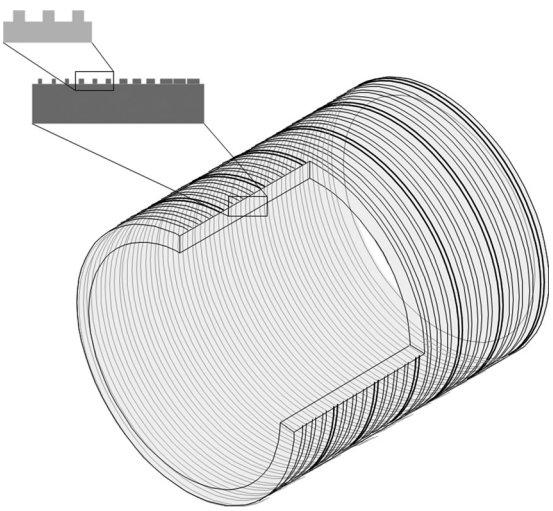

Fig. 8 Sequencing of features on the cylinder surface for experiments. For any resist film thickness, the experiment comprised multiple line arrays (sections) with different substrate speeds. Each speed was applied for three rotations.

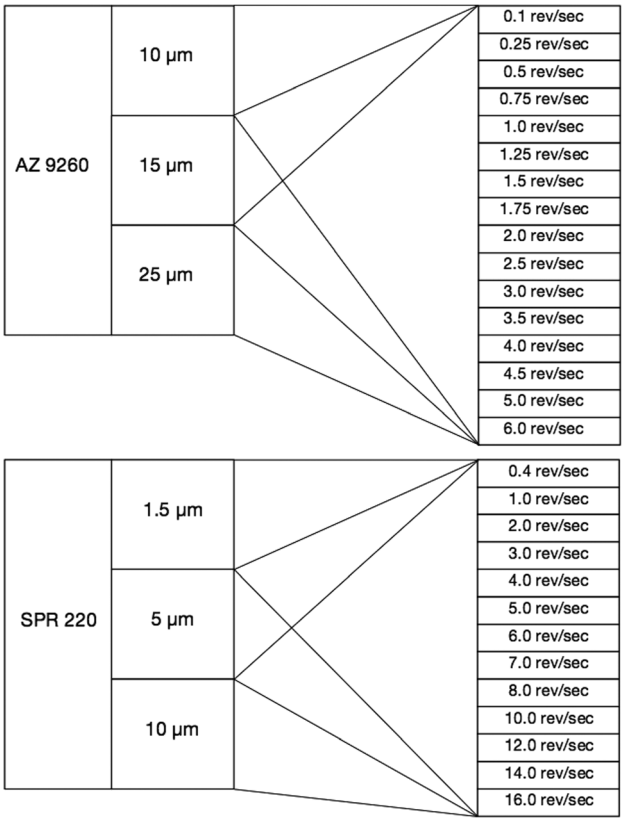

Fig. 9 Table of experiments for different speeds and film thicknesses for both photoresists AZ 9260 and SPR 220

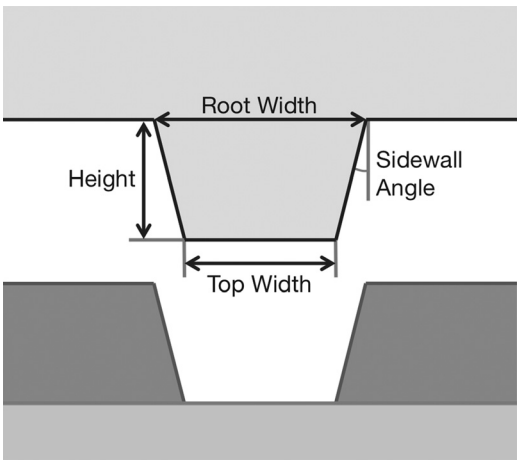

Fig. 10 Feature cross section dimensions. Note that the top width will be the corresponding printing surface for the stamp.

the model, the higher contrast AZ 9260 resist does indeed produce steeper sidewalls than SPR 220.

Medium Contrast Resist (SPR 220). The experiments were conducted using SPR 220-3.0 with a medium viscosity, thinned with a 2:1 solution of ethyl lactate (Sigma Aldrich, St. Louis, MO) and anisole (Sigma Aldrich, St. Louis, MO). Following exposure, the pattern was developed using MF-24A developer (Dow Corning, Midland, MI).

Figure 12 shows the result for SPR 220 with different substrate speeds and a film thickness of 5 μm. Each data point represents the average of 60 measurements comprising all three angular locations for each of 20 bands spaced over the center region of the

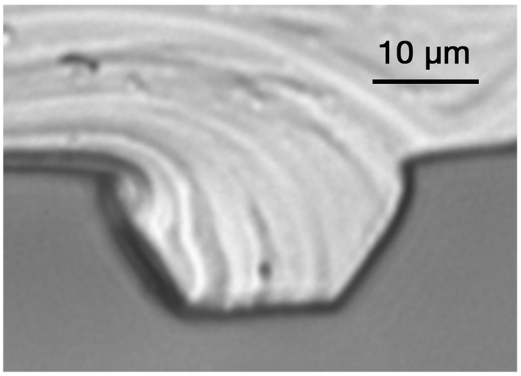

(a)

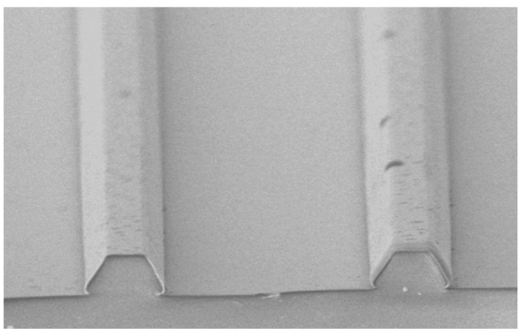

(b)

Fig. 11 Cross section of stamp features produced on AZ 9260 master with 12 μm feature height and 12 μm feature width at the top. (*a*) Microscope picture of cross section and (*b*) ESEM picture of same stamp.

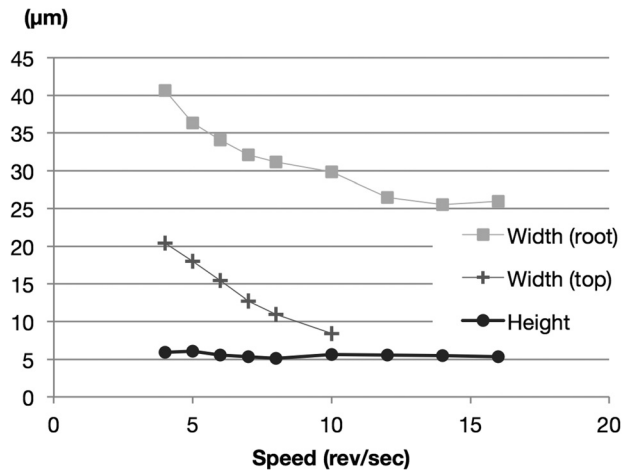

Fig. 12 Width and height of features formed in SPR 220 (thickness 5 μm). Burning or dual-tone effects were visible at speeds lower than 10 rev/s, creating a narrow process window.

cylinder. As expected, the height is constant over all dose levels, indicating exposure through the full thickness of the resist. Moreover, a constant and substantial dependence of the root and top width on the speed (∼1/dose) is noted, along with a nearly constant difference between these two. This indicates a nearly constant sidewall angle, which is evident in the cross section shown in Fig. 13.

It is important to note that SPR 220 showed considerable effects of dual-tone behavior or burning upon over-exposure. Once a threshold exposure dose is reached, the state of the material turned from soluble to insoluble again, showing a "dented" topology in the resulting stamp. Finally, the exposure of SPR 220 was not

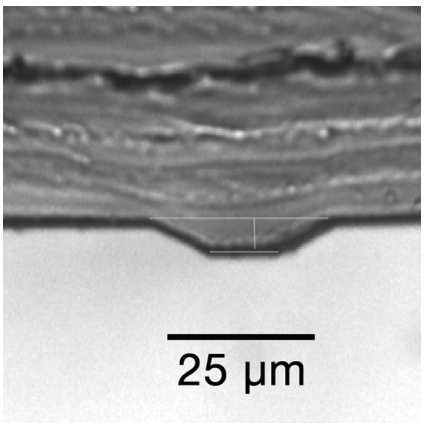

Fig. 13 Typical stamp created with a SPR 220 pattern. With SPR 220, straight but highly angled sidewalls were formed. The image above shows the features formed for 8 rev/s. At the printing side, the feature of the stamp has a width of 11 μm at a total height of 5.1 μm.

fully rate invariant in that faster exposure times required reduced energy dose.

The experiments confirmed that for increasing substrate speed and thus decreasing energy dose, the width of the produced feature decreases. Below a certain threshold dose, the cross-sectional shape of the formed feature did not reveal a flat top with distinct edges at the sidewalls, but instead a round feature. However, the height of the feature did not immediately decrease, indicating that the SU-8 layer (that is, full feature height) was still reached.

High-Contrast Resist (AZ 9200). AZ 9200 is a thick-film photoresist recommended for film thicknesses usually between 5 and 25 μm. The resist was chosen since it is known to produce a good contrast and precise edges (provided the optional postexposure bake is omitted). The feature sizes for both 12 and 18 μm film thicknesses are shown in Fig. 14. For a given film thickness, the exposure dose determined the size of the features. Below a threshold dose, no feature was produced, which is typical of a high-contrast resist. It is worth noting that increasing the volume of resist and thus increasing the film thickness does not reduce the

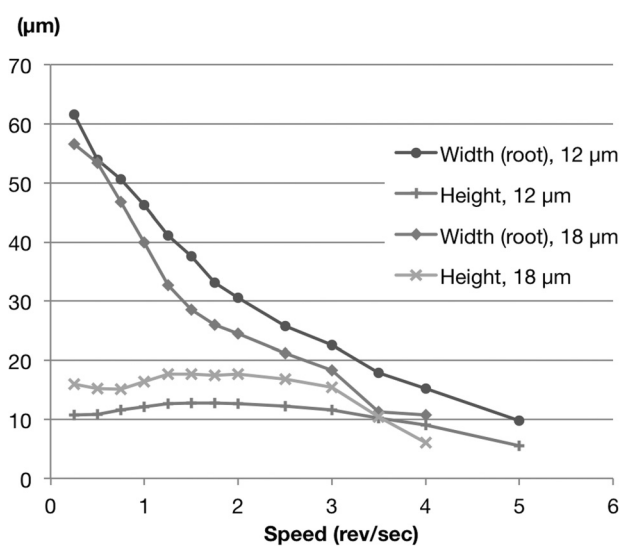

Fig. 14 Feature height and width comparison for different film thicknesses in AZ 9260. For an increase in speed (a decrease in dose), the width of the feature decreases as expected. The height data indicate that both low and high dose can lead to a decrease in feature height.

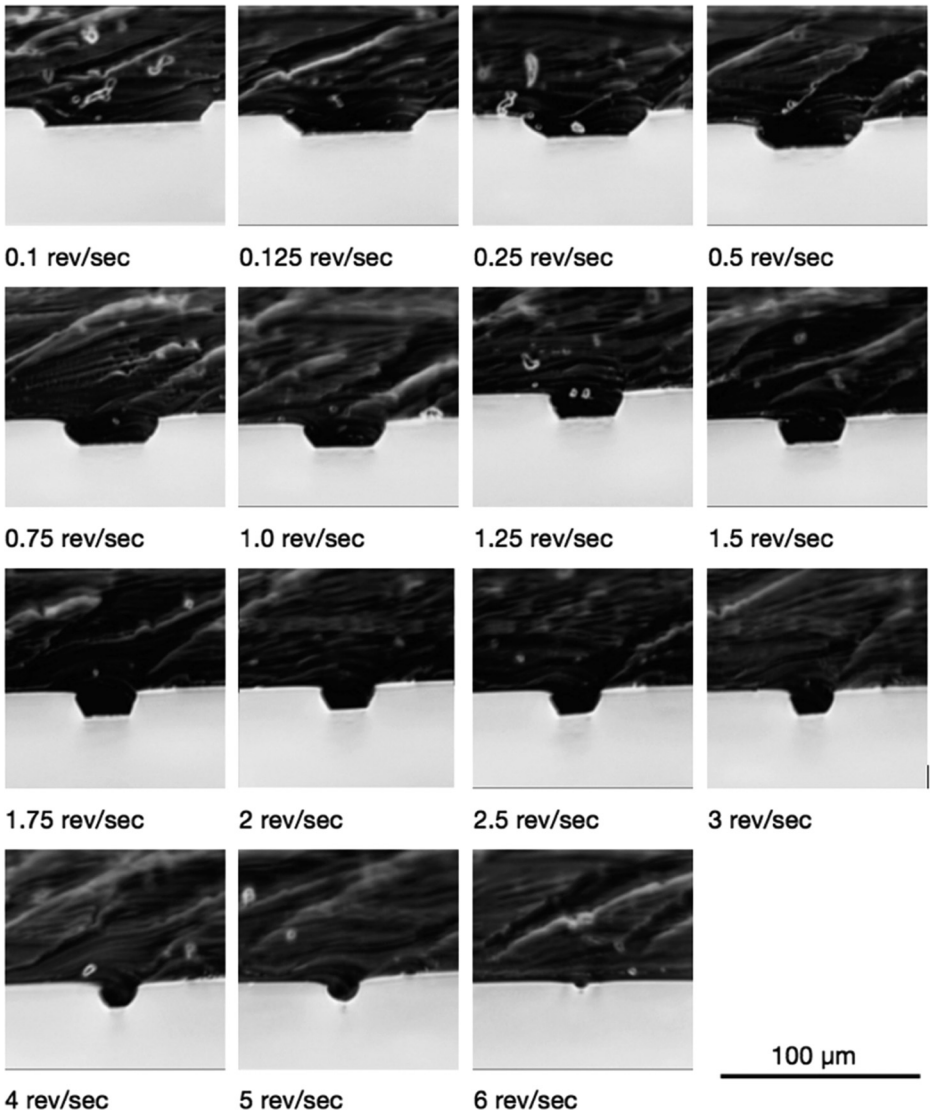

Fig. 15 Effect of speed on feature cross section for AZ 9260. Increasing writing speed reduces local energy dose and thus feature width. Note that for low speeds, the sidewalls of the features are formed by the edge of the Gaussian laser beam, resulting in a quality loss, and that for high speeds the resist threshold is not met to produce a full feature down to the substrate layer. These images were taken in a sample with 13 μm pattern thickness.

minimum root width. It can also be seen that when too little or too much energy is applied, the feature height decreases, and that in the speed range between 1.2 rev/s and 2.5 rev/s the feature depth is constant at the expected height.

AZ 9260 was more robust to overexposure effects. A higher exposure dose increased the feature width until adjacent features merged, and a width range up to 100 μm could be observed in thicknesses below 10 μm without burning or dual-tone effects. In higher thicknesses, the resist burned before reaching the exposure dose necessary to expand the reaction further to either side of the incoming beam.

As the dose decreased, the width decreased in nearly a linear fashion, while the sidewall shape remained nearly constant. This effect is illustrated with cross sections of a stamp taken at different substrate speeds (the inverse of dose levels) as shown in Fig. 15.

Process Variation. The apparatus used for these experiments uses a linear stage to position the laser and optics parallel to the axis of rotation of the drum. The laser is fixed on the stage and can be manually adjusted in both its height and angle relative to the axis of motion of the stage for initial alignment and focus. The optics, comprising a lens and a mirror, and the motor-driven centrifuge are mounted on three-ball kinematic couplings. However, it was found that axial alignment errors of the laser beam relative to the centrifuge cylinder strongly influenced the resulting feature shape. From Fig. 16, it is evident that both the resist thickness and the focus of the laser were variable. While these effects are problematic for implementation, they are fortuitous here since they illustrate the effect of varying the focus location. As this figure illustrates, the morphology of the feature is shown to change as the location of the focus moves from below to above the nominal top surface location. While it was not possible to measure the focus change directly, it was noted that the observed geometry change is in accordance with Mack [23]. Varying the location of the focused laser beam waist results in a variation of both peak intensity and standard deviation of the input Gaussian beam at the surface and at any other location along its axis. This was indicated by either a more sharply defined feature (section 1) or a comparatively underdeveloped one (section 10).[3]

[3]It should be noted that the system was focused manually at a location near the outlet (for visual access) by minimizing the spot size on the surface of the resist.

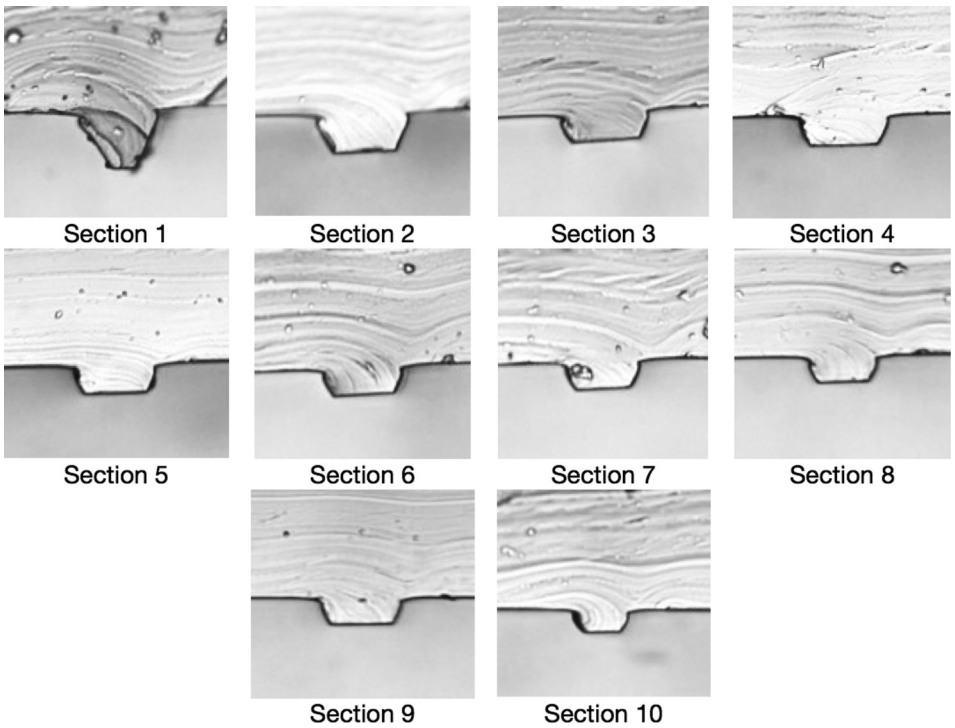

Fig. 16 Feature cross sections at different axial locations for a fixed substrate speed of 2 rev/s (i.e., a fixed dose). As the laser moves from the inner most to outermost location, the effect of variable focus produces a variable morphology in a nominal 10 μm thick AZ 9260 layer.

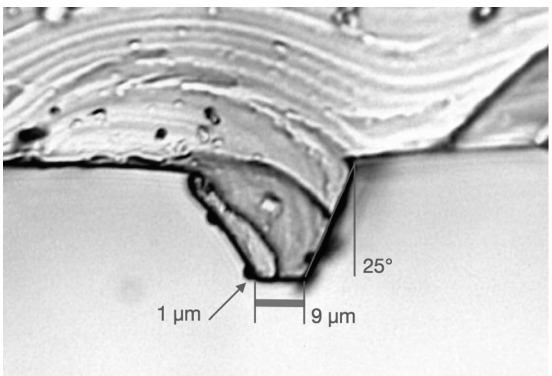

Fig. 17 Cross-sectional geometry optimized for μCP. With a feature height of 20 μm, a root width of 25 μm, and a top width of 9 μm, a sidewall angle of 25 deg is achieved.

Cross-Sectional Shape Control Implications

Whereas conventional photolithography is primarily interested in steep sidewalls for subsequent etching steps, the μCP process benefits from a sidewall geometry that makes the features mechanically robust. By simply making the base of the feature wider than the top (printing) width, thereby creating a sloped sidewall, the mechanical stability of the features is greatly enhanced.

An example is shown in section 1 of Fig. 16. This feature, shown in greater detail in Fig. 17, has an actual printing surface of 9 μm with a root width of 25 μm and feature height of 20 μm. This leads to a sidewall angle of 25 deg from vertical. If the sidewalls were vertical, the resulting feature would have an aspect ratio of about three and would be very prone to buckling collapse. However, applying the analysis conducted by Darbandi et al. [25] to this shape, the taper in this feature would have an equivalent buckling load more than eight times as high as a feature 9 μm wide and 20 μm tall without the taper.

Another dominant mode of collapse occurs when the region between features deforms into contact with the substrate owing to excessive overall stamp pressure. This effect can greatly limit the allowable sparsity and spacing of features in a stamp and thus limit the feasible patterns. However, a series of numerical simulations by Hizir et al. [18] of a deformable stamp with properties typical of PDMS demonstrated that even at large feature spacing, the effect of a tapered sidewall is significant. For the cross section of Fig. 17, it was found that allowable roof collapse pressures could increase up to 25% for sidewall angles of 45 deg regardless of feature spacing.

The present work illustrates that the sidewall angle can be varied both by choice of resist and the shape of the laser beam. A most notable observation is that high contrast resist, normally associated with steep sidewalls, can create a sidewall slope that has very beneficial properties when used in tools for μCP.

Simulation Accuracy and Extension to General Patterning

The simulation based on the Dill photoresist model has been shown to model the process characteristics well and in particular shows excellent prediction fidelity for sidewall contour. In particular, it captures the effect of different resist contrasts (see Fig. 18) and the effect of variable dose levels. It can also be used to examine the effect of overlapping beam paths to determine minimum feature spacing and to examine boundaries of the feature width achievable in raster scanning.

For general stamp patterning either a vector or raster-scanning method can be used. Given the need to carefully control the dose (typically by travel speed), the former method is preferred, since the latter depends on the response of the resist to successive passes of the laser. To move relative to the substrate in an arbitrary direction at a given speed, however, motion axes need to meet specific requirements regarding speed and acceleration (e.g., the linear stage of the presented apparatus does not support these requirements.) To enable raster scanning, the laser must be

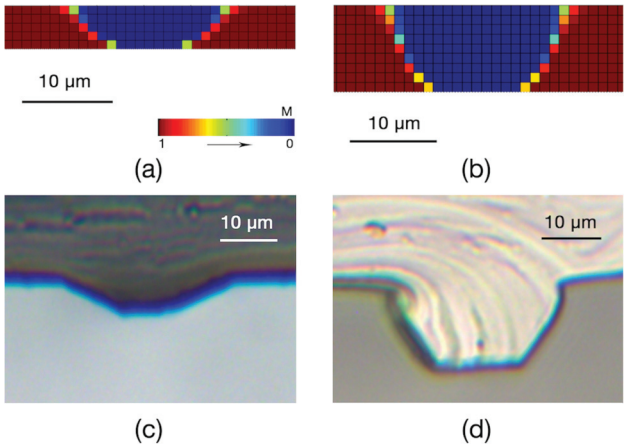

Fig. 18 Simulation versus experimental results for SPR 220 and AZ 9260

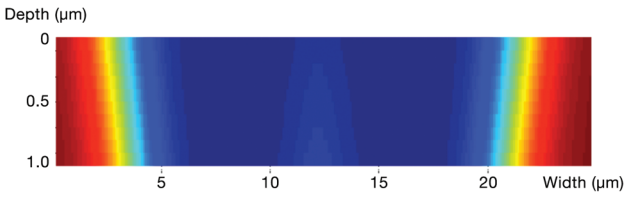

Fig. 19 Simulated effect of beam overlap for AZ 9260. Both passes were with a 5 μm beam, and the second pass was offset by 10 μm. The result was a total width of 19 μm with fully developed root geometry on both sides.

precisely registered on the cylinder both axially and circumferentially, and turned on and off at the appropriate relative position. An extreme example would be axial lines, which would require pulsing the laser at identical angular displacements (on successive rotations) while translating axially to create overlapping arcs of the desired width.

Simulations were performed to see if features much larger than the beam width could be produced on the same resist by successive exposure of adjacent material, as realized in raster scanning. Figure 19 shows that overlapping beams with an offset can be used to create features with variable width and sidewall contours unchanged from single passes.

It should be noted, however, that the simplified model of the beam geometry to a constant focus combined with the 2D representation did not allow for precise intensity calibration nor for modeling changes in energy distribution along the laser axis. If necessary, an improvement could be achieved by incorporating Mack's work [24] into the simulation to provide for the effect of the beam geometry.

Extending the simulation in this way would allow for simulating configurations with a significantly reduced depth of focus, hence increased sensitivity to focal displacement. This would allow examining the minimum feature size for a given resist thickness. Commercial software is available that incorporates these effects, such as OPTOLITH (Silvaco, Santa Clara, CA) or PROLITH (KLA Tencor, Milpitas, CA), which is largely based on Mack's work.

Such a simulation can also be used to extend the results to a greater variety of potential cross-sectional shapes by using multiple passes of beams with different widths, for example, a first pass with a narrow beam that is followed by a much wider beam that will only partially penetrate the cross section (or vice versa), thereby creating highly stable printing features.

Conclusions

The process of patterning a cylindrical photoresist film using a scanned laser was investigated both computationally and experimentally. Two kinds of DNQ-based photoresists of differing contrast were tested in their ability to present a patterning material for continuous μCP stamps. They were compared in their capacity to provide for a robust process and their capacity to create a mold for high-resolution, high-fidelity stamp features. This allowed for examining the scope of a novel direct-write process for the centrifugal casting of cylindrical tools for μCP.

The new method examined in this work allows for the production of seamless, cylindrical μCP tools made from PDMS using direct-write photolithography. Further, this work elucidates the means to vary the shape of the feature sidewalls using this method, in order to enhance mechanical stability of these features when subjected to print force variation. This capability is gained through (1) the creation of a predictive model of the photolithographic process using MATLAB and (2) the verification of this model with the thick-film photoresistive polymers SPR 220 and AZ 9200. Greater precision and process robustness can be achieved in the subsequent printing process with such a tool by adding the capacity to control the cross section of the stamp features.

Adding mechanical stability to the tooling is an important step in the scaling of μCP toward a continuous roll-to-roll process. In addition, the method of wafer-less tool fabrication was shown to enable the creation of seamless cylindrical tools that are not limited by silicon wafer sizes. Hence, this work shows a way toward large-scale, high throughput μCP, enabling a manufacturing process for high-precision surface patterning on a large, industrial scale.

Acknowledgment

The authors would like to thank the King Fahd University of Petroleum and Minerals (KFUPM) in Dhahran, Saudi Arabia, for funding the research reported in this paper through the Center for Clean Water and Clean Energy at Massachusetts Institute of Technology (MIT) and KFUPM.

References

[1] Biebuyck, H. A., Larsen, N. B., Delamarche, E., and Michel, B., 1997, "Lithography Beyond Light: Microcontact Printing With Monolayer Resists," IBM J. Res. Dev., **41**(1.2), pp. 159–170.
[2] Xia, Y., and Whitesides, G. M., 1998, "Soft Lithography," Ann. Rev. Mater. Sci., **28**(1), pp. 153–184.
[3] Xia, Y., Qin, D., and Whitesides, G. M., 1996, "Microcontact Printing With a Cylindrical Rolling Stamp: A Practical Step Toward Automatic Manufacturing of Patterns With Submicrometer-Sized Features," Adv. Mater., **8**(12), pp. 1015–1017.
[4] Rogers, J. A., Bao, Z., Makhija, A., and Braun, P., 1999, "Printing Process Suitable for Reel-to-Reel Production of High-Performance Organic Transistors and Circuits," Adv. Mater., **11**(9), pp. 741–745.
[5] Lee, H. H., Menard, E., Tassi, N. G., Rogers, J. A., and Blanchet, G. B., 2004, "Large Area Microcontact Printing Presses for Plastic Electronics," MRS Online Proc. Libr., **846** (published online).
[6] Stagnaro, A., 2008, "Design and Development of a Roll-to-Roll Machine for Continuous High-Speed Microcontact Printing," M.Eng. thesis, Massachusetts Institute of Technology, Cambridge, MA.
[7] Datar, C. A., 2009, "Design and Development of High Precision Elastomeric-Stamp Wrapping System for Roll-to-Roll Multi-Layer Microcontact Printing," M.Eng. thesis, Massachusetts Institute of Technology, Cambridge, MA.
[8] Petrzelka, J. E., and Hardt, D. E., 2013, "Laser Direct Write System for Fabricating Seamless Roll-to-Roll Lithography Tools," Proc. SPIE, **8612**, pp. 8612-1–8612-14.
[9] Petrzelka, J. E., and Hardt, D. E., 2012, "Static Load-Displacement Behavior of PDMS Microfeatures for Soft Lithography," IOP J. Micromech. Microeng., **22**(7), p. 075015.
[10] Hui, C. Y., Jagota, A., Lin, Y. Y., and Kramer, E. J., 2002, "Constraints on Microcontact Printing Imposed by Stamp Deformation," Langmuir, **18**(4), pp. 1394–1407.
[11] Perl, A., Reinhoudt, D. N., and Huskens, J., 2009, "Microcontact Printing: Limitations and Achievements," Adv. Mater., **21**(22), pp. 2257–2268.
[12] Delamarche, E., Schmid, H., Michel, B., and Biebuyck, H., 1997, "Stability of Molded Polydimethylsiloxane Microstructures," Adv. Mater., **9**(9), pp. 741–746.
[13] Ruiz, S. A., and Chen, C. S., 2007, "Microcontact Printing: A Tool to Pattern," Soft Matter, **3**(2), pp. 168–177.
[14] Abgrall, P., and Nguyen, N.-T., 2009, *Nanofluidics*, Artech House, Norwood, MA.

[15] Lipomi, D. J., Martinez, R. V., Cademartiri, L., and Whitesides, G. M., 2012, "7.11: Soft Lithographic Approaches to Nanofabrication," Polym. Sci. Compr. Ref., **10**, pp. 211–231.
[16] Chaudhury, M. K., and Whitesides, G. M., 1991, "Direct Measurement of Interfacial Interactions Between Semispherical Lenses and Flat Sheets of Poly (dimethylsiloxane) and Their Chemical Derivatives," Langmuir, **7**(5), pp. 1013–1025.
[17] Menard, E., and Rogers, J. A., 2010, "Stamping Techniques for Micro- and Nanofabrication," *Springer Handbook of Nanotechnology*, Springer, New York, pp. 313–332.
[18] Hizir, F. E., Al-Qahtani, H. M., and Hardt, D. E., 2014, "Deformation of Stamp Features With Slanted Walls During Microcontact Printing," COMSOL Conference, Boston, MA.
[19] Dill, F. H., Hornberger, W. P., Hauge, P. S., and Shaw, J. M., 1975, "Characterization of Positive Photoresist," IEEE Trans. Electron Devices, **22**(7), pp. 445–452.
[20] Swinehart, D. F., 1962, "The Beer-Lambert Law," J. Chem. Educ., **39**(7), pp. 333–335.
[21] Schilling, A., Herzig, H. P., Stauffer, L., Vokinger, U., and Rossi, M., 2001, "Efficient Beam Shaping of Linear, High-Power Diode Lasers by Use of Micro-Optics," Appl. Opt., **40**(32), pp. 5852–5859.
[22] Sun, H., 2012, *Laser Diode Beam Basics, Manipulations and Characterizations*, Springer Science & Business Media, Medford, MA.
[23] Mack, C. A., 2007, *Fundamental Principles of Optical Lithography: The Science of Microfabrication*, Wiley, Hoboken, NJ.
[24] Nietner, L., 2014, "A Direct-Write Thick-Film Lithography Process for Multi-Parameter Control of Tooling in Continuous Roll-to-Roll Microcontact Printing," S.M. thesis, Massachusetts Institute of Technology, Cambridge, MA.
[25] Darbandi, S. M., Firouz-Abadi, R. D., and Haddadpour, H., 2010, "Buckling of Variable Section Columns Under Axial Loading," J. Eng. Mech., **136**(4), pp. 472–476.